Published online 22 October 2011 *Nucleic Acids Research, 2012, Vol. 40, No. 4* ***1485–1498***
doi:10.1093/nar/gkr868

FANCJ coordinates two pathways that maintain epigenetic stability at G-quadruplex DNA

Peter Sarkies[1], Pierre Murat[2], Lara G. Phillips[1], K.J. Patel[1], Shankar Balasubramanian[2,3,4] and Julian E. Sale[1,*]

[1]Medical Research Council Laboratory of Molecular Biology, Hills Road, Cambridge, CB2 0QH, [2]Department of Chemistry, University of Cambridge, Lensfield Road, Cambridge, CB2 1EW, [3]Cancer Research UK, Cambridge Research Institute, Li Ka Shing Centre, Cambridge, CB2 0RE and [4]School of Clinical Medicine, The University of Cambridge, Cambridge, CB2 0SP, UK

Received August 2, 2011; Revised September 23, 2011; Accepted September 29, 2011

ABSTRACT

We have previously reported that DT40 cells deficient in the Y-family polymerase REV1 are defective in replicating G-quadruplex DNA. *In vivo* this leads to uncoupling of DNA synthesis from redeposition of histones displaced ahead of the replication fork, which in turn leads to loss of transcriptional repression due to failure to recycle pre-existing repressive histone post-translational modifications. Here we report that a similar process can also affect transcriptionally active genes, leading to their deactivation. We use this finding to develop an assay based on loss of expression of a cell surface marker to monitor epigenetic instability at the level of single cells. This assay allows us to demonstrate G4 DNA motif-associated epigenetic instability in mutants of three helicases previously implicated in the unwinding of G-quadruplex structures, FANCJ, WRN and BLM. Transcriptional profiling of DT40 mutants reveals that FANCJ coordinates two independent mechanisms to maintain epigenetic stability near G4 DNA motifs that are dependent on either REV1 or on the WRN and BLM helicases, suggesting a model in which efficient *in vivo* replication of G-quadruplexes often requires the established 5′–3′-helicase activity of FANCJ acting in concert with either a specialized polymerase or helicase operating in the opposite polarity.

INTRODUCTION

Maintaining epigenetic memory through somatic cell division is of critical importance in preserving stable gene expression and cell identity. Propagation of this memory is proposed to require the preservation of histone post-translational modifications, despite the fact that cell division requires incorporation of newly synthesized histones lacking the modifications characteristic of chromatin found at active or repressed genes [reviewed in (1)]. However, histone modifications linked to transcriptional states can be copied from parental to newly synthesized nucleosomes through the ability of chromatin modifying complexes to recognize the modification that they themselves introduce (2–4) suggesting that, following replication, the newly incorporated histones could be modified to reflect the pre-existing state of the parental histones [reviewed in (1,5)]. This model places stringent requirements on the continuity of replicative DNA synthesis as new histones must be deposited concurrently with parental histone recycling in order to maintain the registration between the histone code and underlying DNA sequence. Without this coordination, parental histones will not be deposited near to their original locations and the information carried by their post-translational modifications may therefore be lost.

Continuous DNA synthesis is challenged by replication impediments caused by exogenous DNA damaging agents, endogenous sources of DNA damage and structured DNA, all of which can cause replicative polymerases to pause or stall. Due to the inherent danger that a collapsed fork poses to genomic integrity, numerous proteins converge on stalled replication forks to protect them and enable rapid resumption of DNA synthesis [reviewed in (6)]. One important pathway to promote the resumption of continuous DNA replication is translesion synthesis, during which low fidelity polymerases of the Y-family bypass DNA damage thereby allowing conventional processive polymerases to continue replication [reviewed in (7)]. Importantly, bypass can take place at one of two temporally distinct points relative to histone

*To whom correspondence should be addressed. Tel: +44 1223 252941; Fax: +44 1223 412178; Email: jes@mrc-lmb.cam.ac.uk

displacement by the advancing replicative helicase. The first possibility is for the helicase to run ahead and for replication to restart downstream of the blockage, leaving a gap that can be filled in later on. This appears to be the dominant approach used by budding yeast (8). It is dependent on the ubiquitination of the sliding clamp PCNA by Rad6/Rad18, which recruits TLS polymerases or promotes recombination to assist in gap filling (9). PCNA ubiquitination-dependent gap filling also operates in vertebrate cells but does so alongside a second pathway operational at the replication fork, which is dependent on the unusual Y-family DNA polymerase REV1 (10,11). The deoxycytidyl transferase REV1 possesses a second, non-catalytic function that serves to recruit other TLS polymerases to the replication fork via its interaction with them (12) and the sliding clamp PCNA (13). Thus, in the absence of REV1, cells depend more heavily on gap-filling to complete replication of damaged DNA templates (10).

REV1 is also involved in replicating undamaged DNA at sequences capable of forming G-quadruplex secondary structures (14). G4 DNA motifs, of the general sequence L_{1-7}-G_{3-5}-L_{1-7}-G_{3-5}-L_{1-7}-G_{3-5} (where L can be any base), can form a range of secondary structures at physiological pH and salt concentrations that comprise stacks of four planar Hoogsteen-bonded dG bases coordinated by monovalent metal ions (15,16). G4 DNA motifs are abundant in the vertebrate genome but do not appear to be randomly distributed, instead being found more frequently in the vicinity of promoters as well as at telomeres and in the immunoglobulin loci. There is increasingly strong evidence that these structures form *in vivo* and that they can significantly influence processes such as replication and transcription [reviewed in (17,18)]. Our previous data supports a model in which lack of REV1 leads to the interruption of processive replication at G-quadruplex structures. In turn this leads to uncoupling of DNA synthesis from recycling of parental histones at these sites, resulting in biased incorporation of newly synthesized histones lacking repressive modifications, and a loss of silencing in a subset of genes. (14).

As noted above, many proteins besides REV1 are important in maintaining replication fork integrity in response to replication stress. In particular, several DNA helicases active at the replication fork have also been implicated in processing G-quadruplex structures. FANCJ, deficiency of which gives rise to the human disease Fanconi anaemia (19), is recruited to stalled replication forks following DNA damage (20,21) but is also capable of unwinding G-quadruplex structures *in vitro* (22,23) and has been implicated in preventing deletions at G4 DNA motifs *in vivo* (24,25). The RecQ helicases mutated in Werner syndrome (WRN) and Bloom syndrome (BLM) are also capable of unwinding G-quadruplex structures (26–29), and play prominent roles in the response to replication stress [reviewed in (30)]. Therefore a logical question is whether REV1 acts alone in defending epigenetic stability at G4 DNA motifs or whether it collaborates with specialized helicases.

Here, we show that lack of REV1 also leads to silencing of a subset of G4 DNA motif-containing transcriptionally active loci. We also demonstrate that similar G4 DNA motif-associated epigenetic instability is seen in mutants of FANCJ, WRN and BLM helicases and further establish that FANCJ operates in two independent pathways for replicating G4 DNA motifs that depend on either REV1 or on WRN and BLM acting redundantly to each other. Our data suggest a model in which the ability to replicate G-quadruplex structures in a manner that preserves epigenetic information often requires the concerted action of enzymes acting at both the 5′- and 3′-end of the structure.

MATERIALS AND METHODS

DT40 strains culture and transfection

DT40 cells were cultured as previously described (31). The creation of the *fancj* line used in this study is described in Supplementary Figure S1. The *wrn*/*blm* double mutant was made by targeting the *BLM* locus in the $WRN^{-/-}$ (*wrn*) cells described previously (32). The origin of the other mutants used is listed in Supplementary Table S1.

Chromatin immunoprecipitation and antibodies

The method for ChIP (chromatin immunoprecipitation) and antibodies to H3K4me3, H4K9/14ac, H4 N-terminal tail ac and H3 have been described previously (14). H3K9me2 was immunoprecipitated using 20 µl anti-H3K9me2 from Cell Signalling Technology (Cat. No. 9753). In all cases the specific ChIP signal was normalized to total H3 and then to the signal at the promoter of the constitutively active *GAS41* gene.

q-PCR and qRT–PCR

This was performed as previously described (14). Primers used are listed in Supplementary Table S5.

NMR spectroscopy

^{1}H NMR spectra of CD72-F and BU1A-F were recorded at 25°C using a 500 MHz Bruker Avance 500 TCI spectrometer equipped with a cryogenic TCI ATM probe. The oligonucleotides were annealed in a 10 mM phosphate buffered saline (PBS) buffer (pH 7.0) supplemented with 70 mM KCl and 10% D_2O at a final concentration of 0.1 mM for CD72-F and 0.2 mM for BU1A-F.

Circular dichroism spectroscopy

Circular dichroism (CD) experiments were conducted on a Chirascan spectropolarimeter using a quartz cuvette with an optical path length of 1 mm. Oligonucleotide solutions were prepared at a final concentration of 10 µM in 10 mM lithium cacodylate (pH 7.2) containing 1 mM of ethylenediaminetetraacetic acid (EDTA) and 100 mM of MCl (where M is either Li, Na or K). The samples were annealed by being heated at 95°C for 10 min and slowly cooled to room temperature. Scans were performed over the range of 200–320 nm at 20°C. Each trace is the result of the average of three scans taken with a step size of 1 nm, a time per point of 1 s and a bandwidth of 1 nm. A blank sample containing only buffer was treated in the same

manner and subtracted from the collected data. The data were finally zero corrected at 320 nm.

Replicating plasmid assay

The basis and method for this assay have been described previously (14,33). Briefly, the efficiency of replication is ascertained by comparing the number of *Escherichia coli* colonies generated by transformation of a DpnI-treated Hirt supernatant of the G4 DNA motif-containing plasmid, which is ampicillin resistant, compared with a control plasmid that is kanamycin resistant recovered 24 h after transient transfection into the indicated DT40 line.

Microarrays and data analysis

Microarray experiments were performed using total RNA and the Affymetrix Chicken Genome array, with three repeats using independently isolated RNA for each mutant and for wild-type (WT) DT40. Data was processed using RMA to give $\log_2$ of probe intensity for each repeat, as described previously (14). The principal component analysis (PCA) was carried out on these data using XLSTAT. Probes which showed a change of >0.25 $\log_2$ units relative to the mean WT probe intensity, with a P-value of >0.05 (t-test), were identified as being statistically significantly altered. Macros written in Excel were used to identify genes co-regulated between different mutants. Significance for these overlaps was calculated using the hypergeometric distribution (stattrek.com/Tables/Hypergeometric.aspx). Codirectionality was also identified using Excel macros, and the significance of this was calculated using the χ^2 test, with the expected values assuming complete independence for the mutants calculated using conditional probability. In order to determine the association of G4 DNA motifs to each gene set, a sample of 80–150 genes were randomly selected from the set and the coordinates, with 1500 bp either side of the transcription unit, were downloaded from Ensembl using Biomart. These coordinates were fed into Ensembl's genome browser, to which the coordinates of G4 DNA motifs had been uploaded from www.quadruplex.org, allowing the number of G4 DNA motifs within this window to be counted. The presence or absence of at least one G4 DNA motif, as well as the total number, were compared to a control set of genes whose expression did not change in any of the mutants.

Bu1a staining

Cells were washed in PBS and stained for 30 min at 4°C with anti-Bu1a (also known as chB6) directly conjugated with phycoerythrin (Santa Cruz clone 5K98, Cat. No. 70447) at a 1:10 dilution. Cells were then washed twice in PBS and resuspended in 500 µl PBS before being analyzed by flow cytometry using an LSRII cytometer (Becton–Dickinson). Although ligation of chb6/Bu-1 has previously been shown to induce apoptosis in DT40 (34), staining with this antibody did not induce apoptosis and cloning of Bu-1a-positive was achieved with the same efficiency as Bu1a-negative clones. DT40, being derived from an F1 hybrid bird, is heterozygous for Bu1a and Bu1b (35). To carry out fluctuation analysis single cells staining positive for Bu1a were sorted using a MOFLO (Dako-Cytomation) sorting cytometer and grown for 3 weeks before staining and analysis using flow cytometry as above.

RESULTS

Rev1-deficient DT40 cells exhibit deactivation of G4 DNA motif-containing genes, as well as derepression

We previously showed that *rev1* DT40 cells exhibit derepression of a subset of genes, which correlated to the presence of G4 DNA motifs in the vicinity of their promoters (14). However, global analysis of gene expression in *rev1* and WT DT40 revealed that there are an equal number of genes deactivated in *rev1* relative to WT (Figure 1A and Supplementary Table S2). The dysregulated genes harbour a significant ($P = 0.005$) increase in the number of G4 DNA motifs relative to a control set of genes that were not perturbed in *rev1* cells (Table 1).

Loss of chromatin marks in the CD72 locus is associated with transcriptional deactivation

To investigate this phenomenon further, we initially focused on one gene, CD72, which we identified as being deactivated in *rev1* cells from microarray data (Supplementary Table S2), an observation confirmed by Quantitative reverse transcription PCR (qRT–PCR) from an independent *rev1* line (Figure 1B). CD72 is a transmembrane C-type lectin expressed constitutively on pro- to mature B cells (36). Examination of the *CD72* locus in the vicinity of the promoter revealed three G4 DNA motifs, one of which is in the correct orientation to uncouple replication and histone recycling through the promoter (Figure 1C).

This G-rich sequence contains five runs of 3–4 dGs, separated by potential loops of 3–7 bases [5′-**GG**GACAT**GGG**ACAGAGA**GGGG**TGAGGTT**GGG**CT**GG**]. Biophysical studies on this 37mer oligonucleotide confirmed G-quadruplex formation by the following observations: (i) clearly resolved G-tetrad imino resonance peaks in the ^{1}H NMR spectrum (37) (Figure 1D). Imino protons of guanines (N1-H) are exchangeable with protons of the solvent during an NMR experiment in water. In a typical nucleic acid, when a guanine is unpaired, no peaks related to these protons are observable on the NMR spectra due to rapid exchange. When these protons are involved in any H-bonds, the exchange is slowed and some resonance peaks can be observed. In G:C Watson–Crick base pairs, imino protons appears lower field to 12.7 parts per million (ppm). In Hoogsteen hydrogen bond alignments, imino protons appear between 10.6 and 12 ppm. By accounting for the number of imino resonances for the particular sequence it is possible to ascertain if there are various species in solution and their relative populations. The ^{1}H NMR spectrum of CD72-F reveals 12 resolved peaks in the range 10.8–12.2 ppm (gray shaded area) characteristic of a single conformation of quadruplex in solution. (ii) A reversible hypochromic

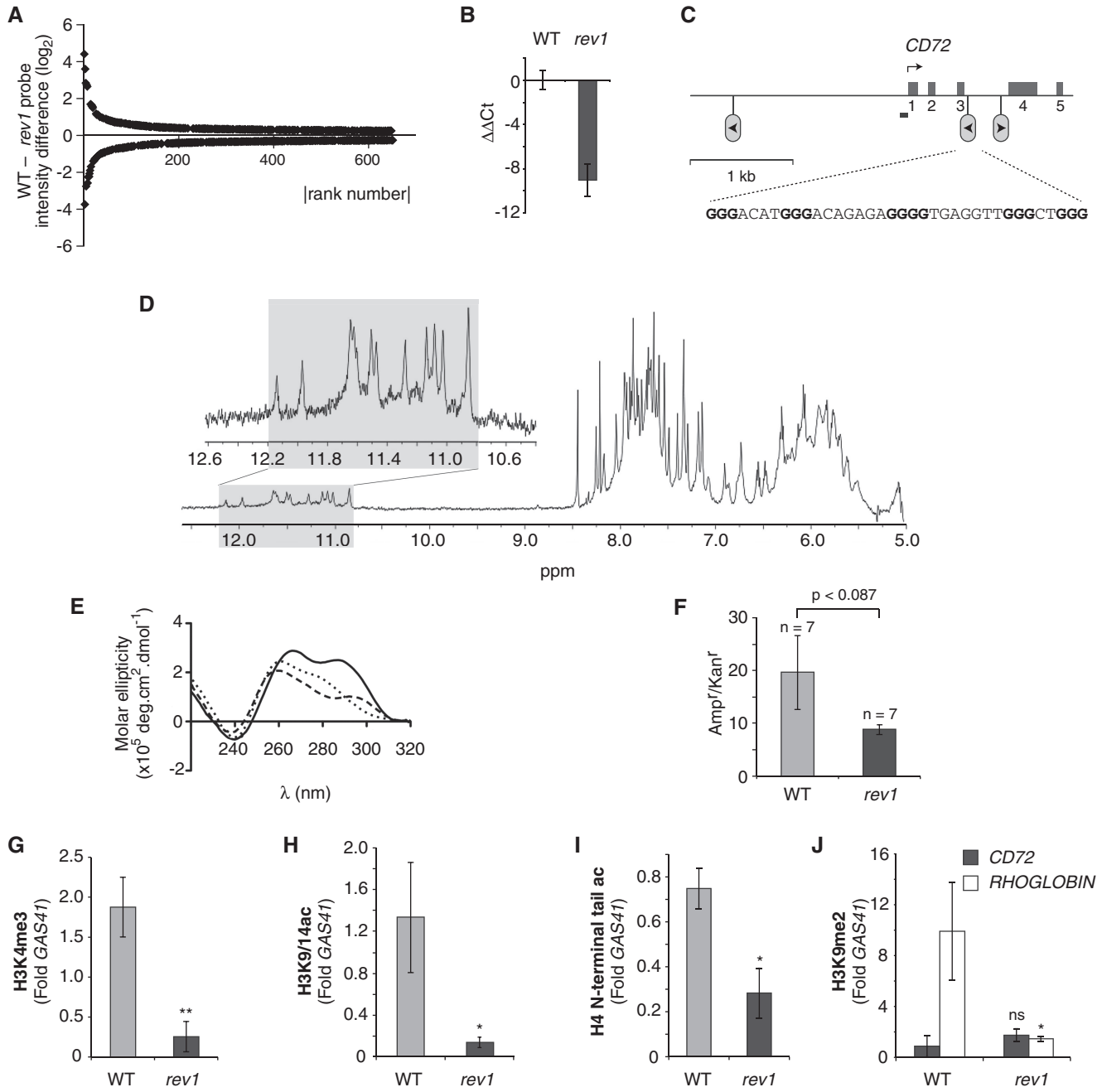

Figure 1. Epigenetic instability in the *CD72* locus of *rev1* cells. **(A)** Plot of probe intensity differences between *rev1* and WT ranked by absolute value (for probes whose expression is altered by >0.25 $\log_2$ with $P < 0.05$). **(B)** qRT-PCR confirming reduction of CD72 expression in a *rev1* line independent of that used in the microarray analysis. Error bars show standard deviation. $P < 0.05$ (2-tailed T-test). **(C)** Map of the *CD72* locus. The first five exons are shown as mid-gray boxes and the positions of the three G4 DNA motifs as inverted lollipops. The arrowhead within the lollipop indicates the direction that a replication fork would have to be travelling for the G-quadruplex structure to form on the leading strand template. The G4 DNA sequence (CD72-F) in the correct orientation to stall replication in *rev1* cells is shown, with the dG repeats in bold. The position of the amplicon generated by the ChIP primers (*CD72*promF & R) is shown as a bar. **(D)** Part of the ^{1}H NMR spectra of CD72-F. In the inset: an expansion of the spectrum focusing on the imino protons of the guanines involved in a tetrad (gray shaded area). **(E)** CD spectrum of CD72-F recorded in the presence of LiCl (dotted line), NaCl (dashed line) and KCl (solid line). **(F)** Replication efficiency of CD72-F incorporated into the leading strand template of the replicating plasmid pQ, shown as the ratio of Amp^r to Kan^r *E. coli* colonies. Amp^r plasmid contains the CD72-F oligo while Kan^r plasmid does not (14). The error bars represent standard error of the mean. *P*-value calculated with the unpaired *t*-test. **(G)** Trimethylation of H3K4 at the *CD72* promoter in WT and *rev1* cells. **(H)** Acetylation of H3K9 and K14 at the *CD72* promoter in WT and *rev1* cells. **(I)** Acetylation of the H4 N-terminal tail at the *CD72* promoter in WT and *rev1* cells. **(J)** Dimethylation of H3K9 at the *CD72* and *RHOGLOBIN* promoters in WT and *rev1* cells. Error bars in F–I represent standard error of the mean; *P*-values compared to WT (one-tailed, unpaired *t*-test): ns = not significant, $*P < 0.075$, $**P < 0.01$.

Table 1. Association of dysregulated genes with G4 DNA motifs

	Control	*rev1*	*fancj*	*rev1/fancj*	*wrn/blm*	*rev1 and wrn/blm*	*fancj and wrn/blm*
Fraction of genes with ≥1 G4 DNA motif	0.69	0.85	0.88	0.83	0.85	0.83	0.77
n	135	93	130	116	164	80	141
P		0.0013	0.0002	0.0075	0.0013	0.036	0.135
G4 DNA motifs per gene	2.63	4.29	3.78	4.18	3.15	4.79	3.31
P		0.005	0.0003	0.0059	0.0186	0.0053	0.03

G4 DNA sequences were identified in the gene body plus 1 kb upstream using pre-existing annotations of the chicken genome in ENSEMBL uploaded from www.quadruplex.org. Genes were selected on the basis of an increase or decrease in probe intensity by ≥0.25 $\log_2$ units with $P < 0.05$. The control set comprises randomly selected probes that exhibit no change between WT and any of the mutants.

melting transition at 295 nm (Supplementary Figure S2A), suggesting formation of an intramolecular structure. The high rate of melting used, 1°C/min, leads to a reversible melting curve which supports the formation of an intramolecular quadruplex. Indeed at this rate and this oligonucleotide concentration, 10 μM, the melting of intermolecular quadruplexes has been shown to be kinetically irreversible (38). (iii) Cation dependent melting temperatures in the order $K^+ > Na^+ > Li^+$ (39) (Supplementary Figure S2A and Supplementary Table S3A) and (iv) a characteristic thermal difference spectrum (40) (Supplementary Figure S2C). Its melting temperature of 59.5°C in the presence of K^+ supports its ability to form a stable structure under physiological conditions (Supplementary Table S2A). CD spectroscopy (Figure 1E and Supplementary Table S3B) was indicative of the formation of a hybrid quadruplex with both parallel and anti-parallel features (41).

We have previously shown that REV1 is required for efficient replication of a G4 DNA motif when placed on the leading strand template (14). To examine whether this was also the case for the *CD72* G4 DNA motif, we cloned the sequence into the replicating plasmid pQ (33), placing it so the G-quadruplex structure would form on the leading strand template as previously described (14). The presence of the *CD72* G4 DNA motif resulted in a reduction in the efficiency of recovery of replicated copies of the plasmid from *rev1*-deficient cells relative to WT cells, the borderline significance of which may reflect the heterogeneity of the structure seen in the CD experiments (Figure 1F). Together these results appear analogous to those we obtained for the *RHOGLOBIN* G4 DNA motif (14) and are consistent with a similar underlying model in which interruption of replication by a G-quadruplex structure in the *CD72* locus of *rev1* cells leads to loss of chromatin modifications associated with transcriptional activation.

To test this, we performed ChIP experiments to examine the histone modifications at the *CD72* promoter. Consistent with the association of H3K4me3 with the promoter of active genes (42,43), we observed high levels of this modification at the *CD72* promoter in WT DT40 cells. However, this enrichment was lost in *rev1* cells (Figure 1G). H3K9/14ac, another mark associated with transcriptional activation (44), was also reduced (Figure 1H). Next we examined acetylation of the N-terminal tail of H4. This modification is associated with both transcriptional activation (44) and with newly deposited histones (45,46), which according to our previous results (14) would lead to the levels of this mark being subject to two opposing forces: loss of pre-existing, acetylated H4 associated with the loss of transcriptional activation but gain of newly synthesized H4 bearing the predeposition acetylations at H4K5 and K12 (45,46). We observed that *rev1* cells exhibited a decrease in H4 N-terminal tail acetylation at the *CD72* promoter relative to WT cells (Figure 1I) suggesting that the loss of acetylation of H4 at this locus due to loss of transcriptional activation is not compensated for by the acetylation introduced by new histone incorporation. Importantly, despite observing loss of histone modifications characteristic of active chromatin, we did not detect a significant increase in the level of the repressive modification H3K9me2 (Figure 1J). This suggests that the reduction in expression is caused by a loss of histone modifications associated with active transcription rather than an active silencing process mediated by the introduction of repression-associated marks.

Surface Bu1a staining as a readout for epigenetic instability in DT40 cells

The loss of expression of CD72 in REV1-deficient cells suggested to us a facile assay for epigenetic instability, based on cell surface staining that would provide a more sensitive readout of loss of expression than Quantitative polymerase chain reaction (q-PCR) as small changes within a bulk population would be detected. As no antibody to chicken CD72 was available we sought another B cell surface marker whose locus contained a G4 DNA motif and whose expression we could monitor by flow cytometry. Bu1a is a cell surface receptor expressed on cells derived from the chicken bursa (47). Its locus contains a G-rich region positioned ~3 kb from the transcription start site (Figure 2A). While this region [5′-**GGGCTGGGTGGG**TGCTGTCAA**GGGCTGGG**] contains two potential overlapping G4 DNA sequences, neither is predicted by available servers as both contain a non-dG loop of 9 bp. Nonetheless, an oligonucleotide comprising all five dG repeats was able to form a robust G-quadruplex structure *in vitro*. The UV-melting curves were reversible and display, in the presence of K^+, a transition at 65.5°C, which was suggestive of an intramolecular quadruplex (Supplementary Figure S2B and C; Supplementary Table S3A). ^{1}H NMR revealed seven

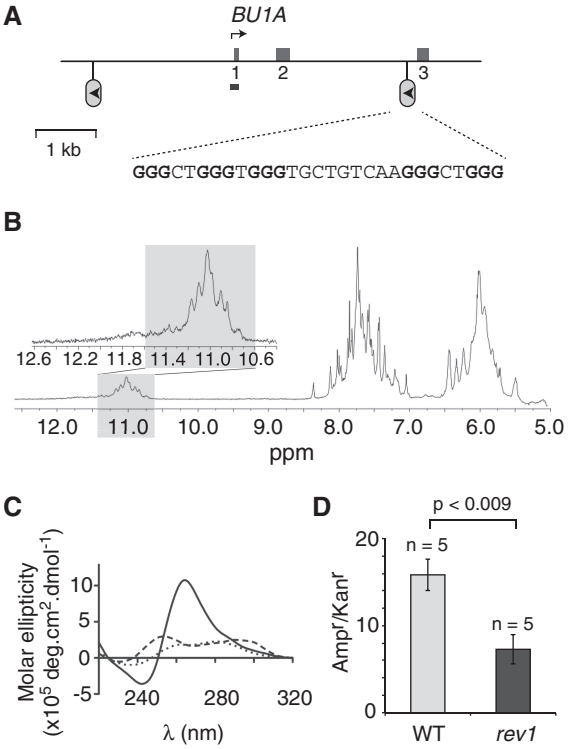

Figure 2. G-quadruplex formation by the G-rich region of the *BU-1 A* locus and its defective replication in *rev1* cells. (**A**) Map of the *BU-1 A* locus. The first three exons are shown as mid-gray boxes. The position of the G-rich region is shown as a lollipop and sequence of the corresponding oligonucleotide BU1A-F shown below. The arrowhead within the lollipop indicates the direction that a replication fork will be travelling in to be stalled by the G-quadruplex in *rev1* cells. The position of the amplicon generated by the ChIP primers (*BU1A*promF & R) is shown as a bar. (**B**) Part of the ^{1}H NMR spectra of BU1A-F. In the inset: an expansion of the spectrum focusing on the imino protons of the guanines involved in a tetrad (gray shaded area). (**C**) CD spectrum of BU1A-F recorded in the presence of LiCl (dotted line), NaCl (dashed line) and KCl (solid line). (**D**) Replication efficiency, in *rev1* cells, of BU1A-F incorporated into the leading strand template of the replicating plasmid pQ, shown as the ratio of Amp^{r} to Kan^{r} *E. coli* colonies. Amp^{r} plasmid contains the BU1A-F oligo while Kan^{r} plasmid does not (14).

broad peaks in the range 10.7–11.3 ppm suggesting conformational exchange between two equivalent quadruplex structures (Figure 2B, gray shaded area). The CD spectrum was characteristic of a parallel stranded G-quadruplex (Figure 2C and Supplementary Table S2B). Further, as for the *CD72* G4 DNA motif, the sequence was replicated less efficiently in *rev1* cells than in WT (Figure 2D).

To assess whether loss of REV1 resulted in instability in Bu1a expression we compared surface expression of Bu1a in *rev1* cells with WT. WT cells exhibit uniformly positive staining for surface Bu1a (Figure 3A). Strikingly, a significant subpopulation of a bulk *rev1* culture exhibited low Bu1a surface staining (Figure 3A). To examine whether Bu1a loss is constitutive during culture, we sorted a population of Bu1a-positive *rev1* by flow cytometry. A population of Bu1a-loss variants could be detected after 24 h and this population had increased by 7 days (Figure 3B). We then cloned single *rev1* cells from the remaining Bu1a-positive population. After 3 weeks expansion we analyzed surface Bu1a levels by flow cytometry and demonstrated that the percentage of Bu1a-loss variants generated in this time varied between clones (Figure 3C), consistent with Bu1a loss being a stochastic process dependent on cell division. Cloning from the Bu1a-loss variant population demonstrated that loss of Bu1a expression was stable and heritable through cell division (Figure 3D). The loss of surface Bu1a in *rev1* cells is associated with decreased mRNA levels (Figure 3E) and further, Bu1a gene expression, as measured by qPCR from different *rev1* clones, correlated to the level of Bu1a surface staining, indicating that the change in surface Bu1a levels is caused by alteration in transcription of the *BU1A* locus (Figure 3F).

Loss of Bu1a expression could be prevented by a transgene driving expression of human REV1 (Figure 3G) as assessed in a fluctuation analysis, in which individual Bu1a-positive clones were propagated for a defined number of divisions. Interestingly, cells expressing a catalytically inactive human REV1 (hREV1$^{[D570AE571A]}$) did not exhibit the same range of Bu1a loss as the *rev1* mutants suggesting a possible role for the catalytic activity of REV1 in the replication of this G4 DNA motif, and in agreement with our previous observations on the *RHOGLOBIN* G4 DNA motif (14). Furthermore, supporting the idea that it is the maintenance of replication fork progression that is essential for maintaining epigenetic stability rather than an ability to carry out lesion bypass *per se*, a DT40 mutant deficient in the ubiquitination of PCNA (*pcna*K164R) (48), and thus in gap-filling pathways of translesion synthesis (10), does not show elevated rates of Bu1a loss (Figure 3G).

We next investigated whether changes in histone modifications were associated with loss of Bu1a expression in *rev1* cells. ChIP analysis of a population sorted for Bu1a-positive cells showed WT levels of active chromatin modifications, while a Bu1a-low population showed reduced H3K4me3, H3K9ac and H4 N-terminal acetylation (Figure 4A–C). Further, there was no significant enrichment of H3K9me2 (Figure 4D). This pattern of histone modification changes is comparable to those seen at the *CD72* locus in *rev1* cells and suggests that a similar mechanism is responsible for the loss of expression. Further, since re-emergence of Bu1a-positive cells from Bu1a-low clones is not observed (Figure 3D), Bu1a loss is a stable epigenetic state.

Together, these data are consistent with loss of the Bu1a surface marker occurring as a result of replication fork stalling at the Bu1a G4 DNA motif, leading to loss of active chromatin modifications and epigenetic instability.

We next examined a range of DT40 DNA repair mutants for Bu1a loss, initially by monitoring Bu1a expression in the bulk population of high passage lines (Figure 5A). In contrast to *rev1* cells, no significant increase in Bu1a loss was seen in lines deficient in the translesion polymerases η or ζ, or in cells defective in proliferating cell nuclear antigen (PCNA) ubiquitination, *rad18* and *pcna*K164R. Additionally, no significant loss was seen in cells lacking the recombination proteins

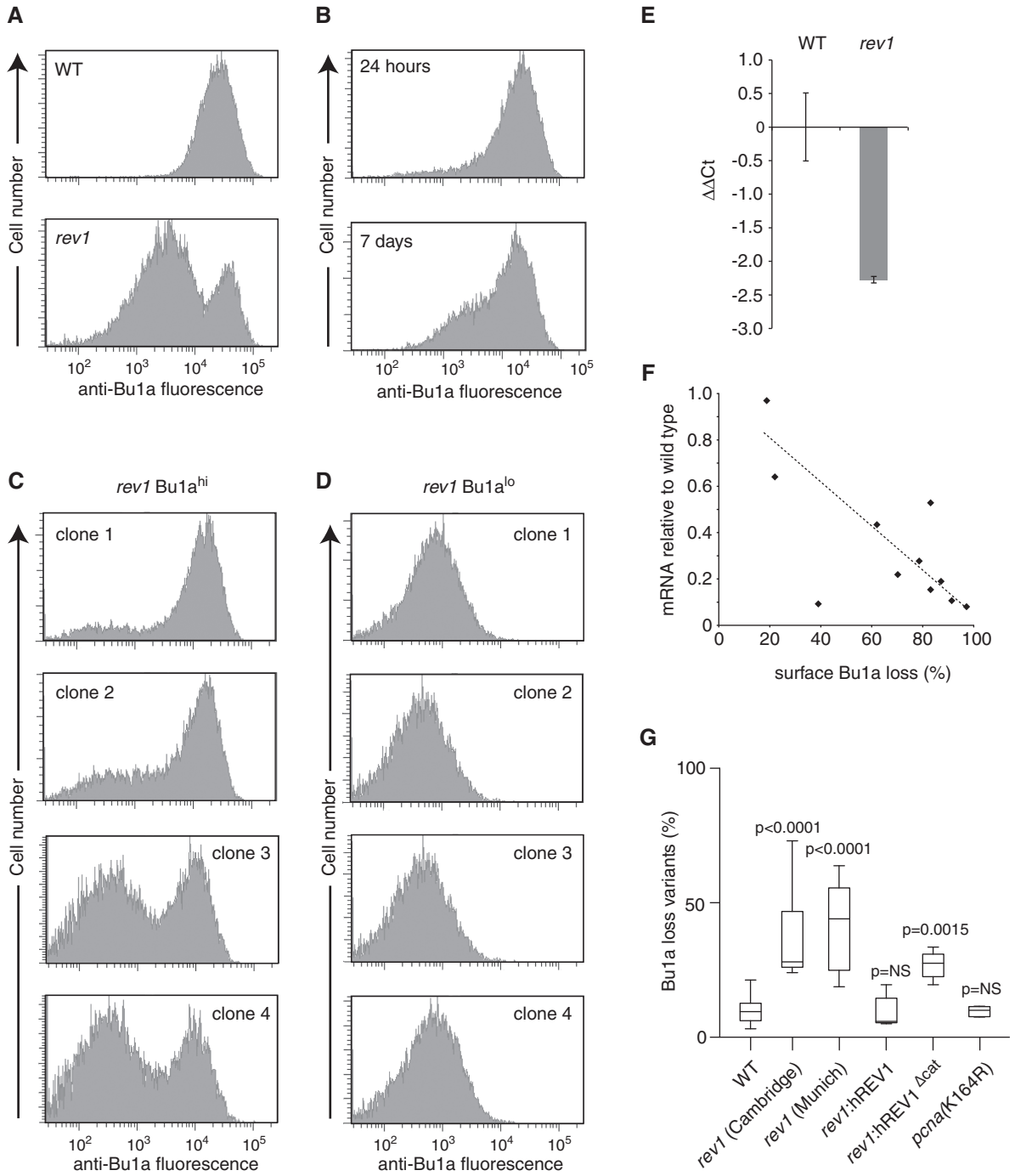

Figure 3. Stochastic loss of surface Bu-1a in *rev1*-deficient cells. (**A**) A high-passage culture of *rev1* cells exhibits a substantial population of Bu1a-loss variants. Flow cytometry histogram showing staining of WT and *rev1* bulk populations with anti-Bu1a. (**B**) Constitutive loss of Bu1a from a Bu1a-positive population of *rev1* cells. *rev1* cells were enriched to >99% Bu1a positive by flow sorting and the population monitored for Bu1a loss at 24 h and 7 days. (**C**) Stochastic loss of Bu1a in Bu1a-positive subclones. Clones were expanded for 3 weeks before analysis by flow cytometry. (**D**) Bu1a loss is a stable phenotype. Expression of Bu1a in selected Bu1a-loss variant clones expanded for 3 weeks. (**E**) Reduction in Bu1a transcript in *rev1* cells. qRT-PCR for Bu1a mRNA. Error bars show standard deviation. $P = 0.05$ (2-tailed T-test). (**F**) Loss of surface expression of Bu1a correlates with decreased mRNA. mRNA level in *individual rev1* clones (WT = 1) assessed by qRT-PCR plotted against the percentage of cells showing negative surface Bu1a expression. (**G**) Complementation of the constitutive loss of Bu1a in *rev1* cells by expression of full length, but not catalytically inactive hREV1. Individual Bu1a-positive subclones of each indicated genotype were expanded for 3 weeks and assessed for Bu1a loss by flow cytometry. *rev1*(Cambridge) and *rev1*(Munich) are two independently generated *rev1* lines (Table S1). For each condition the graph shows the median (central line), range (whiskers) and interquartile range (boxes). The probability (Mann–Whitney U-test) that the distribution of loss is the same as WT is shown. NS = not significantly different. P for the difference between *rev1*:hREV1 and *rev1*:hREV1$^{\Delta cat}$ = 0.0104.

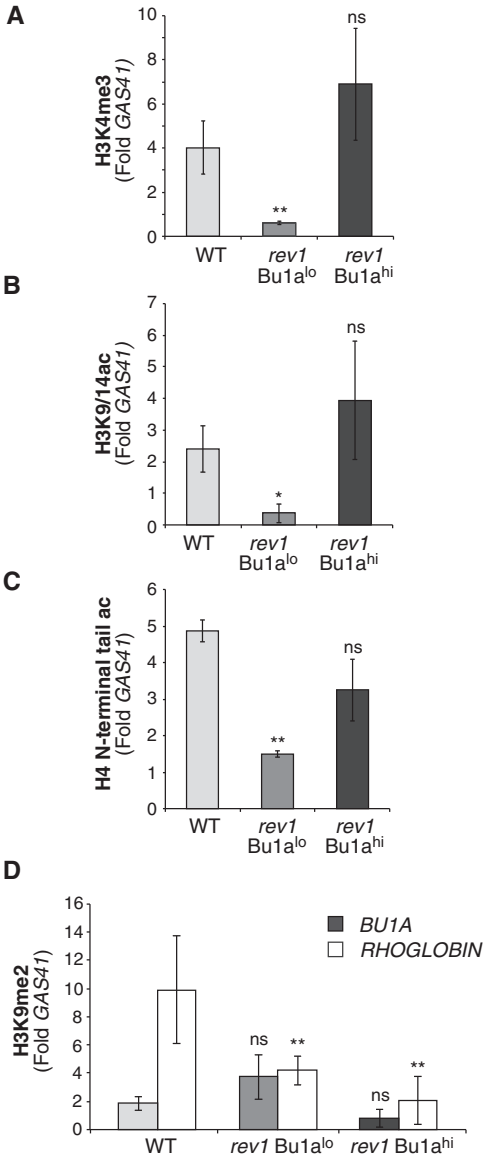

Figure 4. Loss of Bu1a expression gene of *rev1* cells correlates with loss of histone modifications associated with transcriptional activation. (**A**) Trimethylation of H3K4 at the *BU1A* promoter in WT, Bu1a-negative *rev1* cells (Bu1a^{lo}) and *rev1* cells enriched for expression of surface Bu1a (Bu1a^{hi}). (**B**) Acetylation of H3K9 and K14 at the *BU1A* promoter. (**C**) Acetylation of the H4 N-terminal tail at the *BU1A* promoter (**D**) Dimethylation of H3K9 at the *BU1A* (gray bars) and ρ-*GLOBIN* (white bars) promoters in WT, Bu1a-negative *rev1* cells (Bu1a^{lo}) and *rev1* cells enriched for expression of surface Bu1a (Bu1a^{hi}). Error bars represent standard error of the mean, *P*-values compared to WT (one-tailed, unpaired *t*-test): ns = not significant,*$P < 0.075$, **$P < 0.01$.

XRCC3 and RAD54 or in a mutant for the key excision repair factor XPA.

Epigenetic instability in fancj mutants is associated with G4 DNA motifs and is independent of the Fanconi anaemia core complex

We then turned our attention to helicases implicated in G-quadruplex processing. Interestingly, a mutant deficient in the FANCJ helicase exhibited a striking loss of Bu1a expression (Figure 5A), which we confirmed in a fluctuation analysis (Figure 5B). Ongoing Bu1a loss could be prevented by expression of a human FANCJ transgene (Figure 5B). However, this role for FANCJ appears to be independent of the Fanconi anaemia core complex [reviewed in (49)] as a *fancc* mutant exhibited no significant increase in Bu1a loss compared to WT cells (Figure 5A and B). Thus, FANCJ could be involved in preventing epigenetic instability at G4 DNA motifs in a similar manner to REV1. Consistent with this idea, we also found a marked reduction in the expression of the CD72 gene in *fancj* mutants together with a corresponding decrease in H3K4me3 and H3K9/14ac, but no increase in H3K9me2 at the *CD72* promoter (Supplementary Figure S3). Unexplained reproducibly poor recovery of even the control pQ plasmid from *fancj* cells (data not shown) precluded direct analysis of the requirement for FANCJ in G-quadruplex replication.

To confirm the association between altered gene expression and G4 DNA sequences we carried out genome-wide transcriptional profiling of *fancj* cells and identified probes whose mean signal intensity was increased or decreased in each mutant by >40% (>0.25 $\log_2$ units) relative to WT with a $P < 0.05$. This analysis revealed a large number of genes (7152 probes) that exhibit dysregulated expression in the *fancj* mutant (Figure 5C). These genes were significantly associated with G4 DNA motifs compared with an unaffected control set (Table 1). Although loss of FANCJ has been associated with deletions in the vicinity of G-rich sequences (22,24,25), a number of lines of evidence suggest that deletions alone are unlikely to account for the observed dysregulation of gene expression in *fancj* cells. First, we did not detect evidence of deletions around the G4 DNA sequences in *fancj BU1A*- or *CD72*-variants (Supplementary Figures S4 and S5). Second, we did not observe any alteration in the ChIP input signal from the *BU1A* or *CD72* promoters, compared to the control *GAS41* promoter. Third, it might be expected that a significant contribution of deletions to changes in gene expression would result in a bias to decreases in expression across the genome. This is not observed. In *fancj* cells, as for *rev1* (Figure 1A), an equal number of genes show increased expression relative to WT as show decreased expression (Supplementary Figure S6). Finally, it is worth noting that the kinetics of Bu1a loss in *fancj*, and also *rev1*, cells is rapid, such that 30–40% of cells have lost surface Bu1a after 3 weeks. This is much more rapid than even the loss of immunoglobulin gene expression in *fancj* DT40 when augmented by the active mutator activation induced deaminase (AID) (50). Given our failure to detect either deletions or mutations of the *BU1A* locus, and particularly of the G4 DNA motif, it seems unlikely that the observed rate of loss of expression can be accounted for by genetic alterations, though they may make a small contribution.

The WRN and BLM helicases contribute redundantly to the preservation of epigenetic stability

We next examined the contribution of the BLM and WRN helicases, which have also been previously

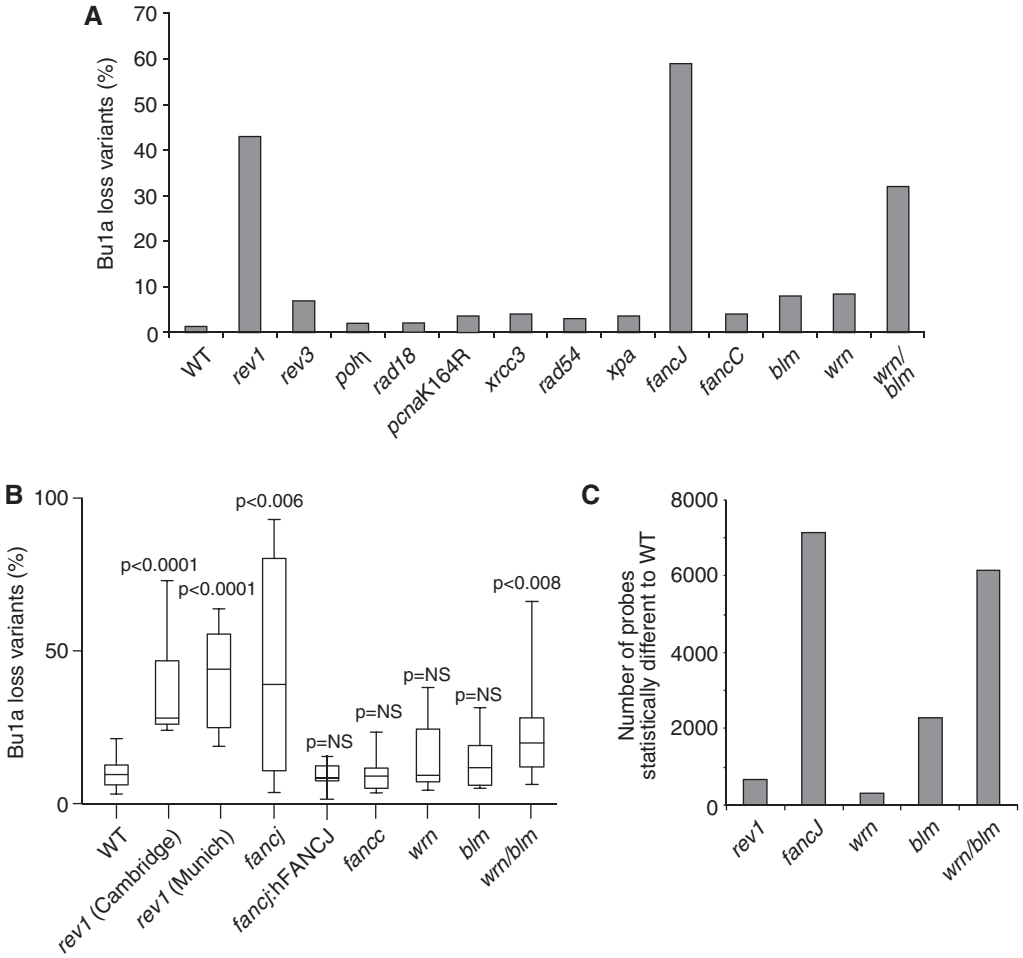

Figure 5. A screen for epigenetic instability. (**A**) Percentage of Bu1a-loss variants in high passage clones of DT40 mutants of the indicated genotype. (**B**) Constitutive instability of Bu1a expression confirmed by fluctuation analysis. Subclones were expanded for 3 weeks after which the percentage of Bu1a-loss variants was determined by flow cytometry. For each condition the graph shows the median percentage Bu1a loss (central line), range (error bars) and interquartile range (boxes). The WT and *rev1* data is reproduced from Figure 4G for comparison. The loss of Bu1a in lines indicated with an asterisk is significantly ($P < 0.01$, Mann–Whitney U-test) different to WT. (**C**) Histogram showing the number of probes statistically significantly perturbed ($P < 0.05$) with a >0.25 log units difference in *rev1*, *fancj*, *wrn, blm, wrn*/*blm* lines compared to WT DT40.

implicated in processing G-quadruplexes (26–29). Neither WRN nor BLM deficient cells showed significantly increased loss of surface Bu1a compared to WT. However, a mutant deficient in both WRN and BLM showed a dramatic increase in the level of Bu1a loss, both in a bulk culture (Figure 5A) and in a fluctuation assay (Figure 5B). Further *wrn*/*blm* double mutants replicated a G4 DNA motif-containing plasmid less efficiently than WT cells (Supplementary Figure S7). The apparent redundancy between WRN and BLM could also be seen in the pattern of genes dysregulated across the genome (Figure 5C). Again the genes dysregulated in each of these mutants are significantly associated with G4 DNA motifs (Table 1), in agreement with a previous report (51). *wrn* cells exhibited relatively little dysregulation of gene expression (304 probes significantly altered compared to WT). While *blm* cells exhibited more dysregulated genes than *wrn* cells (2284 probes), the number of genes whose expression was dysregulated in the *wrn*/*blm* double mutant was much greater than either single mutant (6152 probes). Further, there was a significant overlap both in the identity genes affected and the direction of change of expression between *wrn* and *wrn*/*blm* and *blm* and *wrn*/*blm*, but not between *wrn* and *blm* (Supplementary Figure S8). Together, these data suggest that WRN and BLM are also involved in maintaining epigenetic stability at G-quadruplex forming DNA, but that they act redundantly to each other.

FANCJ collaborates independently with REV1 and with WRN/BLM in maintaining epigenetic stability at G4 DNA motifs

Since *fancj*, *blm* and *wrn*/*blm* mutants exhibited gross alterations in gene expression compared to WT, we carried out principal component analysis (PCA) on the array data from these lines. Intriguingly, we observed that the pattern of gene expression in the *wrn*/*blm* double mutant, rather than resembling the *blm* single mutant, resembles *fancj* (Figure 6A), an observation we confirmed by cluster analysis (data not shown). Combining this with the data from the *BU1A* locus (Figure 5A and B) led us to focus on

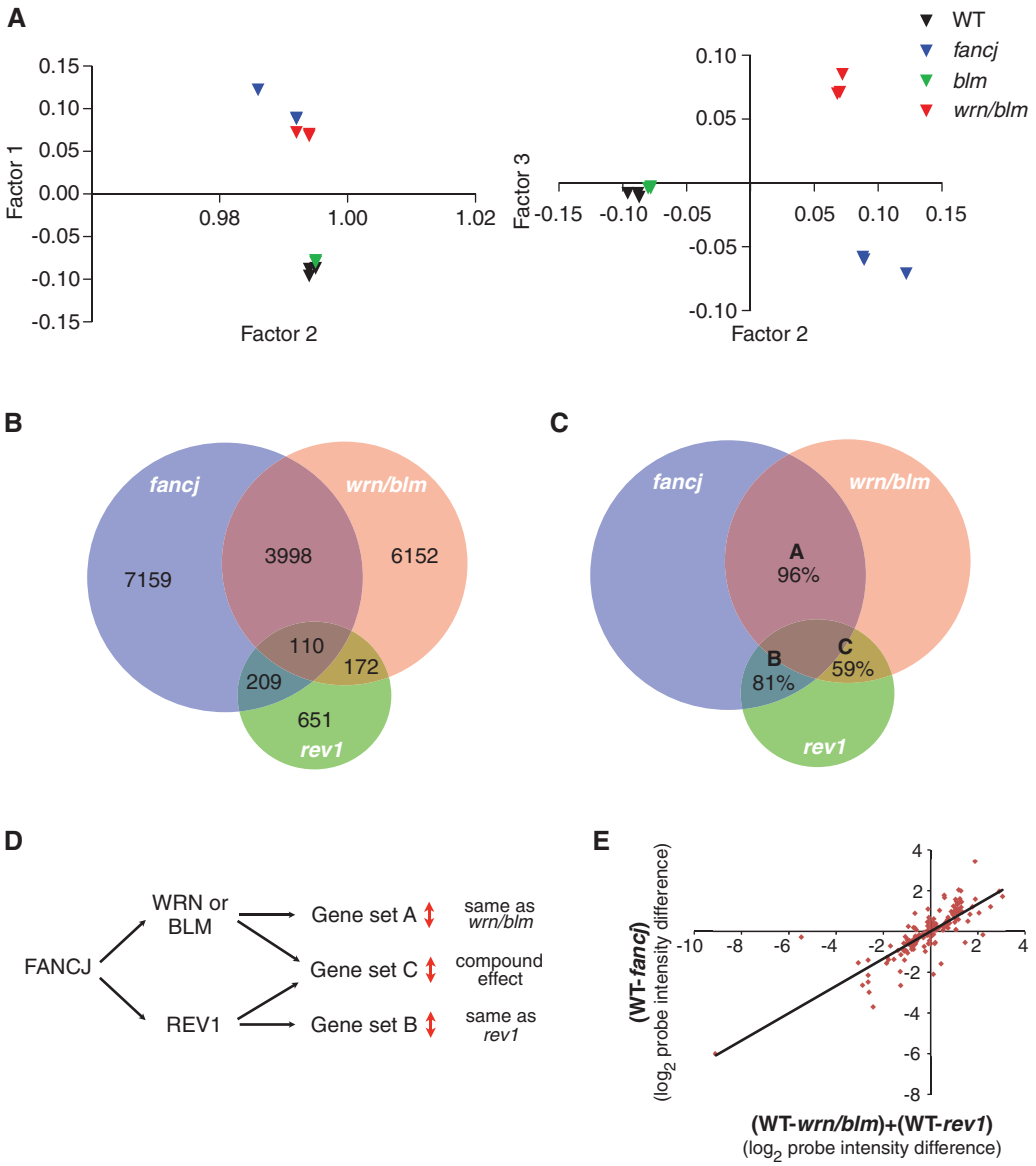

Figure 6. Two pathways for the maintenance of epigenetic stability at G-quadruplex forming DNA sequences. (**A**) PCA on microarray probes from three independently growing *fancj, wrn/blm, blm* and WT DT40 lines. PCA is a statistical method for explaining a complex data set in a minimum number of factors, or principal components. In this case, three orthogonal factors were sufficient to explain >98% of the variation within the data set. (**B**) Venn diagram showing the number of probes statistically significantly perturbed ($P < 0.05$) with a >0.25 log units difference to WT DT40 in *rev1*, *fancj* and *wrn/blm* mutants, and the overlap between these sets. All overlaps are statistically significant (see text). (**C**) Venn diagram as in Figure 7C showing the percentage of probes, within each set, which show the same direction of change in each pair of mutants. The expected codirectionality assuming independence between the conditions is ~50% for each set. (**D**) Hypothetical relationship between FANCJ, WRN or BLM and REV1 in maintaining epigenetic stability. Sets A, B and C refer to the pairwise overlaps between the mutants shown in Figure 6C. (**E**) Changes in probe intensity in the *fancj* mutant for probes overlapping with *rev1* and *wrn/blm*. $\log_2$ change in *fancj* is plotted against the sum of the $\log_2$ change in *rev1* and the $\log_2$ change in *wrn/blm*. The regression line is indicated ($R = 0.82$).

the relationships between the mutants *fancj*, *wrn/blm* and *rev1*.

We examined the overlap between each mutant in terms of which probes were perturbed and the direction of the perturbation, i.e. increased or decreased relative to WT. As predicted by the PCA, the genes dysregulated in *fancj* and *wrn/blm* show a high degree of overlap ($P < 1 \times 10^{-17}$, Fisher's hypergeometric distribution) (Figure 6B). Strikingly, 96% of genes within this overlap set change in the same direction in *fancj* and *wrn/blm* ($P < 1 \times 10^{-17}$, χ^2 test) (Figure 6C), implying that the effect of deleting FANCJ or WRN and BLM is the same on the expression of these genes. There is also an increased propensity for G4 DNA sequences within this set (Table 1) implying that the presence of DNA with G-quadruplex forming potential is likely to underlie the requirement for FANCJ and WRN/BLM in epigenetic stability. At the same time, there is a strong overlap between the genes whose expression is perturbed in *fancj* and in *rev1* ($P < 1 \times 10^{-17}$) (Figure 6B) and again there is a

statistically significant codirectionality relationship ($P < 1 \times 10^{-14}$) (Figure 6C) and an increased propensity for G4 DNA sequences (Table 1). However, the overlap between genes perturbed in *rev1* and *wrn*/*blm*, while still being statistically significant ($P < 1 \times 10^{-12}$) (Figure 6B), does not show the same directionality effect: only 59% change in the same direction, barely above that expected by chance ($P > 0.2$) (Figure 6C). This implies that while there are some genes whose expression is maintained through the action of REV1 and WRN or BLM, the processes involved are distinct.

We wanted to explore the idea of separate pathways for maintenance of epigenetic stability involving REV1 and WRN or BLM in more detail, so we looked at the set of genes that overlapped between the *rev1* and the *wrn*/*blm* double mutants. If FANCJ is involved in separate pathways protecting epigenetic stability at G4 DNA motifs involving either REV1 or WRN/BLM, then the perturbations in *fancj* mutants in this set of genes (set C in Figure 6C) should reflect separate contributions from REV1 *and* from WRN/BLM. Thus, if a gene were to increase by 2-fold in *rev1* and 2-fold in the *wrn*/*blm* double mutant then its expression would be >2-fold increased in *fancj*; equally, if a gene is increased in expression in *rev1* and decreased in *wrn*/*blm* then it may not show an overall change in *fancj*. This predicts that the expression changes seen in this set in *fancj* mutants would be a function of the changes in *rev1* mutants and changes in the *wrn*/*blm* double mutant (Figure 6D). To test this idea, we took the genes falling into set C (Figure 6C) and plotted the $\log_2$ change in *fancj* cells against the sum of the $\log_2$ change in *wrn*/*blm* and the $\log_2$ change in *rev1*. Strikingly, this graph revealed a linear correlation (Figure 6E) suggesting that the effect on gene expression of removing FANCJ is equivalent to the effect of removing both REV1 and WRN and BLM simultaneously. The correlation coefficient of 0.82 is significantly better than that seen between *fancj* and either *wrn*/*blm* or *rev1* individually within gene set C (Supplementary Table S4); moreover, the relationship does not hold outside of gene set C (Supplementary Table S4). These observations strongly reinforce the idea that the REV1 and the WRN/BLM pathways to maintain epigenetic stability at G4 DNA motifs are distinct, but that both involve FANCJ.

DISCUSSION

A neutral state of gene expression?

We previously proposed that the loss of H3K9me2 around the promoter of repressed loci in *rev1* cells is a passive consequence of uncoupling DNA synthesis from histone recycling induced by replication arrest at G-quadruplex structures. Supporting this model we did not observe any increase in the level of marks associated with transcriptional activation (e.g. H3K4me3 and H3K9/14ac) suggesting that there was no active induction of gene expression. The data we present here support an analogous model at active loci: G-quadruplex-induced uncoupling of DNA synthesis and histone recycling leads to the passive loss of active chromatin marks by biased incorporation of new histones. However, there is no active repression of affected loci, evidenced by an increase in H3K9me2. Thus, in cell lines defective for G-quadruplex replication both the derepression of a silent locus and the deactivation of an active locus produce a similar net result: a 'neutral' expression state with neither active nor repressive chromatin present. This model supports the notion that one or more 'active' histone modifications may be *sensu stricto* epigenetic, such that impaired recycling due to replication fork stalling leading to its reduction *directly* impairs the ability of the cell to maintain a transcriptionally active state. Of the 'active' histone modifications, we believe that H3K4me3 is the most likely candidate for an epigenetic mark, due to the long half-life of methylation on histones relative to acetylation (52), and its involvement in heritable gene activation in *Drosophila* development [reviewed in (53)].

Stochasticity of G4 DNA motif-associated epigenetic instability

At the *BU1A* locus we observed stochastic loss of expression over time, consistent with a mechanism involving replication fork stalling at G-quadruplex structures. It is noteworthy that the *BU1A* G4 DNA motif is further away from the transcriptional start site than is observed in *CD72* or *RHOGLOBIN*. The post-replicative gap that would have to be left in order to lead to loss of epigenetic information at the promoter is therefore ~3 kb in length, somewhat larger than the estimated average for human cells of ~0.8 kb (54). However, this is within the range of lengths directly observed in DNA from *Saccharomyces cerevisiae* (8). Moreover, our previously described computer simulation (14) shows that increasing the variance of gap length increases the loss of epigenetic information suggesting that the system is sensitive to rare events in which long gaps are created (Supplementary Figure S9). It is possible therefore that the position of the G4 DNA sequence relative to the transcriptional start site may explain why we were able to successfully isolate single cells with high expression from a population of *rev1* cells that had been grown for several months in culture as loss of Bu1a expression in any particular cell may be a relatively infrequent event.

Collaboration between REV1 and specialized helicases in G-quadruplex replication

Deletion of FANCJ, a helicase that has previously been shown to be able to unwind G-quadruplex structures (22,23), has been linked to deletions in G-rich sequences (22,24,25). We observed changes in gene expression both at the *BU1A* and *CD72* loci, as well as genome wide. As discussed above deletions alone are unlikely to explain all of these effects. Because the set of dysregulated genes correlate significantly with an increased frequency of G4 DNA motifs, secondary effects due to alterations in transcription factors are also unlikely to explain the majority of these changes, though this may make some contribution.

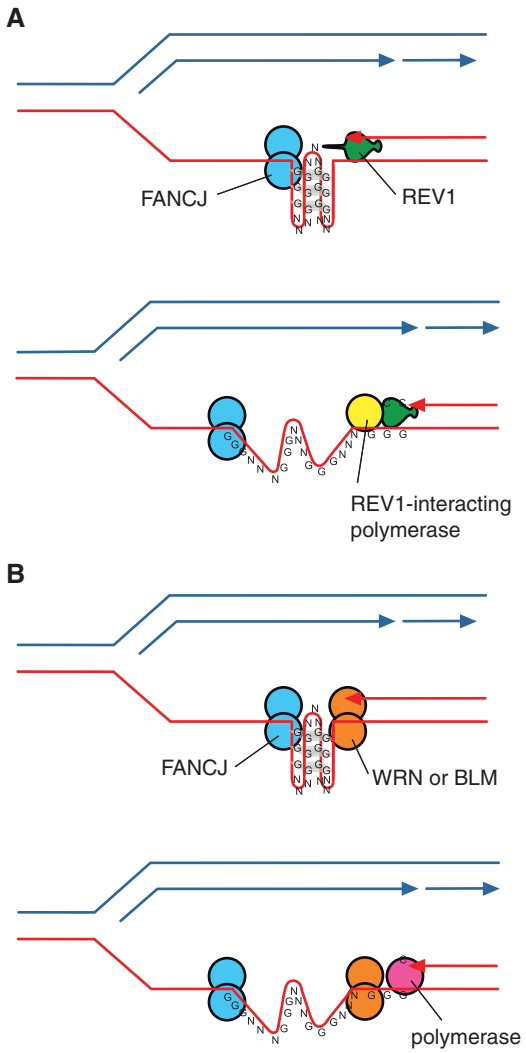

Figure 7. Model for the cooperation of FANCJ with REV1 and with the WRN and BLM proteins in replicating a G-quadruplex. (**A**) Cooperation of FANCJ with REV1. We have previously suggested that REV1 may help destabilize G-quadruplex structures (14). This could facilitate unwinding by FANCJ, which will act from the opposite side of the G-quadruplex structure. (**B**) Cooperation of FANCJ with WRN or BLM. Since the helicase activities of WRN and BLM helicases have the opposite polarity to FANCJ, this suggests a model by which they also act from the other end of the quadruplex, possibly simultaneously with FANCJ. DNA synthesis across the remainder of the G4 DNA sequence may then be affected by one of the replicative polymerases.

The overlap between genes dysregulated in *fancj* and *rev1* cells, and the association of these genes with G4 DNA motifs, also suggests that REV1 is likely to operate with FANCJ at the fork to facilitate the replication of a subset of G-quadruplex-forming sequences. As FANCJ is a 5′–3′-DNA helicase (22,23) this suggests a model in which it acts from the opposite end of the G-quadruplex to new DNA synthesis (Figure 7A).

Using G4 DNA motif-associated dysregulation of gene expression as a readout for effective G-quadruplex replication, we also show redundancy between the RECQ helicases WRN and BLM in maintaining epigenetic stability at G4 DNA motifs. Further, our data suggests that WRN and BLM act with FANCJ but in a different process from that involving FANCJ and REV1. Although WRN and BLM have been implicated in transcriptional regulation (51), they have much more extensively characterized roles in DNA replication [reviewed in (30)]. Therefore, we favour the idea that, as for FANCJ and REV1, this collaboration between FANCJ and WRN/BLM defends epigenetic stability by ensuring continuous replication at G-quadruplex-forming DNA sequences. Consistent with such a model, FANCJ and BLM have been shown to interact physically, and the two colocalize to sites of stalled replication (20). The fact that RECQ helicases act from the 3′–5′-direction suggests that WRN and BLM would access a G-quadruplex in the opposite direction to FANCJ, allowing them to collaborate in facilitating DNA replication through the quadruplex (Figure 7B).

Overall, our results offer a general model for *in vivo* G-quadruplex replication, in which the collaboration between two helicases, or a helicase and a polymerase, approaching from opposite ends of the G-quadruplex structure, could facilitate processive DNA synthesis. Further work will be needed to identify the factors, for instance the structure and sequence context of the G4 DNA motif, that determine which enzyme or combination of enzymes are used, and whether additional helicases and polymerases are involved. Finally, as WRN, BLM and FANCJ are all implicated in human diseases, our work may have significance for understanding the complex organismal phenotypes caused by mutations in these critical guardians of genome stability.

SUPPLEMENTARY DATA

Supplementary Data are available at NAR Online: Supplementary Tables 1–5 (including one Excel workbook), Supplementary Figures 1–9, Supplementary Methods and Supplementary References [55–67].

ACKNOWLEDGEMENTS

We would like to thank Ian McFarlane and his team at the University of Cambridge School of Clinical Medicine Microarray Facility for carrying out the microarray hybridization, Maria Daly and Fan Zhang for cell sorting, Charlie Reams for advice on the Zippee simulation, Shunichi Takeda and Jean-Marie Buerstedde for sharing DT40 lines, Rebekka Schwab and Wojciech Niedzwiedz for the hFANCJ expression construct and Daniela Rhodes and members of the Sale lab for helpful discussions and comments on the article.

FUNDING

Work in J.E.S's lab is supported by the Medical Research Council (MC_US_A024_0039), Association for International Cancer Research (08-0017 & 11-0514) and The Fanconi Anaemia Research Fund. Work in S.B's lab is supported by programme funding from Cancer

Research UK (C9681/A5709). Funding for open access charge: Medical Research Council.

Conflict of interest statement. None declared.

REFERENCES

1. Corpet,A. and Almouzni,G. (2009) Making copies of chromatin: the challenge of nucleosomal organization and epigenetic information. *Trends Cell Biol.*, **19**, 29–41.
2. Bannister,A.J., Zegerman,P., Partridge,J.F., Miska,E.A., Thomas,J.O., Allshire,R.C. and Kouzarides,T. (2001) Selective recognition of methylated lysine 9 on histone H3 by the HP1 chromo domain. *Nature*, **410**, 120–124.
3. Lachner,M., O'Carroll,D., Rea,S., Mechtler,K. and Jenuwein,T. (2001) Methylation of histone H3 lysine 9 creates a binding site for HP1 proteins. *Nature*, **410**, 116–120.
4. Hansen,K., Bracken,A., Pasini,D., Dietrich,N., Gehani,S., Monrad,A., Rappsilber,J., Lerdrup,M. and Helin,K. (2008) A model for transmission of the H3K27me3 epigenetic mark. *Nat. Cell Biol.*, **10**, 1291–300.
5. Margueron,R. and Reinberg,D. (2010) Chromatin structure and the inheritance of epigenetic information. *Nat. Rev. Genet.*, **11**, 285–296.
6. Branzei,D. and Foiani,M. (2010) Maintaining genome stability at the replication fork. *Nat. Rev. Mol. Cell Biol.*, **11**, 208–219.
7. Lehmann,A.R., Niimi,A., Ogi,T., Brown,S., Sabbioneda,S., Wing,J.F., Kannouche,P.L. and Green,C.M. (2007) Translesion synthesis: Y-family polymerases and the polymerase switch. *DNA Repair*, **6**, 891–899.
8. Lopes,M., Foiani,M. and Sogo,J.M. (2006) Multiple mechanisms control chromosome integrity after replication fork uncoupling and restart at irreparable UV lesions. *Mol. Cell*, **21**, 15–27.
9. Hoege,C., Pfander,B., Moldovan,G.L., Pyrowolakis,G. and Jentsch,S. (2002) RAD6-dependent DNA repair is linked to modification of PCNA by ubiquitin and SUMO. *Nature*, **419**, 135–141.
10. Edmunds,C.E., Simpson,L.J. and Sale,J.E. (2008) PCNA ubiquitination and REV1 define temporally distinct mechanisms for controlling translesion synthesis in the avian cell line DT40. *Mol. Cell*, **30**, 519–529.
11. Jansen,J., Tsaalbi-Shtylik,A., Hendriks,G., Gali,H., Hendel,A., Johansson,F., Erixon,K., Livneh,Z., Mullenders,L., Haracska,L. *et al.* (2009) Separate domains of Rev1 mediate two modes of DNA damage bypass in mammalian cells. *Mol. Cell. Biol.*, **29**, 3113–3123.
12. Guo,C., Fischhaber,P.L., Luk-Paszyc,M.J., Masuda,Y., Zhou,J., Kamiya,K., Kisker,C. and Friedberg,E.C. (2003) Mouse Rev1 protein interacts with multiple DNA polymerases involved in translesion DNA synthesis. *EMBO J.*, **22**, 6621–6630.
13. Ross,A.L., Simpson,L.J. and Sale,J.E. (2005) Vertebrate DNA damage tolerance requires the C-terminus but not BRCT or transferase domains of REV1. *Nucleic Acids Res.*, **33**, 1280–1289.
14. Sarkies,P., Reams,C., Simpson,L.J. and Sale,J.E. (2010) Epigenetic instability due to defective replication of structured DNA. *Mol. Cell*, **40**, 703–713.
15. Sundquist,W.I. and Klug,A. (1989) Telomeric DNA dimerizes by formation of guanine tetrads between hairpin loops. *Nature*, **342**, 825–829.
16. Williamson,J.R., Raghuraman,M.K. and Cech,T.R. (1989) Monovalent cation-induced structure of telomeric DNA: the G-quartet model. *Cell*, **59**, 871–880.
17. Lipps,H.J. and Rhodes,D. (2009) G-quadruplex structures: in vivo evidence and function. *Trends Cell Biol.*, **19**, 414–422.
18. Maizels,N. (2006) Dynamic roles for G4 DNA in the biology of eukaryotic cells. *Nat. Struct. Mol. Biol.*, **13**, 1055–1059.
19. Levitus,M., Waisfisz,Q., Godthelp,B.C., de Vries,Y., Hussain,S., Wiegant,W.W., Elghalbzouri-Maghrani,E., Steltenpool,J., Rooimans,M.A., Pals,G. *et al.* (2005) The DNA helicase BRIP1 is defective in Fanconi anemia complementation group J. *Nat. Genet.*, **37**, 934–935.
20. Suhasini,A.N., Rawtani,N.A., Wu,Y., Sommers,J.A., Sharma,S., Mosedale,G., North,P.S., Cantor,S.B., Hickson,I.D. and Brosh,R.M. Jr (2011) Interaction between the helicases genetically linked to Fanconi anemia group J and Bloom's syndrome. *EMBO J.*, **30**, 692–705.
21. Gong,Z., Kim,J.E., Leung,C.C., Glover,J.N. and Chen,J. (2010) BACH1/FANCJ acts with TopBP1 and participates early in DNA replication checkpoint control. *Mol. Cell*, **37**, 438–446.
22. London,T.B., Barber,L.J., Mosedale,G., Kelly,G.P., Balasubramanian,S., Hickson,I.D., Boulton,S.J. and Hiom,K. (2008) FANCJ is a structure-specific DNA helicase associated with the maintenance of genomic G/C tracts. *J. Biol. Chem.*, **283**, 36132–36139.
23. Wu,Y., Shin-ya,K. and Brosh,R.M. Jr (2008) FANCJ helicase defective in Fanconia anemia and breast cancer unwinds G-quadruplex DNA to defend genomic stability. *Mol. Cell. Biol.*, **28**, 4116–4128.
24. Cheung,I., Schertzer,M., Rose,A. and Lansdorp,P.M. (2002) Disruption of dog-1 in Caenorhabditis elegans triggers deletions upstream of guanine-rich DNA. *Nat. Genet.*, **31**, 405–409.
25. Kruisselbrink,E., Guryev,V., Brouwer,K., Pontier,D.B., Cuppen,E. and Tijsterman,M. (2008) Mutagenic capacity of endogenous G4 DNA underlies genome instability in FANCJ-defective C. elegans. *Curr. Biol.*, **18**, 900–905.
26. Fry,M. and Loeb,L.A. (1999) Human werner syndrome DNA helicase unwinds tetrahelical structures of the fragile X syndrome repeat sequence d(CGG)n. *J. Biol. Chem.*, **274**, 12797–12802.
27. Sun,H., Karow,J.K., Hickson,I.D. and Maizels,N. (1998) The Bloom's syndrome helicase unwinds G4 DNA. *J. Biol. Chem.*, **273**, 27587–27592.
28. Mohaghegh,P., Karow,J.K., Brosh,R.M. Jr, Bohr,V.A. and Hickson,I.D. (2001) The Bloom's and Werner's syndrome proteins are DNA structure-specific helicases. *Nucleic Acids Res.*, **29**, 2843–2849.
29. Kamath-Loeb,A.S., Loeb,L.A., Johansson,E., Burgers,P.M. and Fry,M. (2001) Interactions between the Werner syndrome helicase and DNA polymerase delta specifically facilitate copying of tetraplex and hairpin structures of the d(CGG)n trinucleotide repeat sequence. *J. Biol. Chem.*, **276**, 16439–16446.
30. Chu,W.K. and Hickson,I.D. (2009) RecQ helicases: multifunctional genome caretakers. *Nat. Rev. Cancer*, **9**, 644–654.
31. Simpson,L.J. and Sale,J.E. (2003) Rev1 is essential for DNA damage tolerance and non-templated immunoglobulin gene mutation in a vertebrate cell line. *EMBO J.*, **22**, 1654–1664.
32. Phillips,L.G. and Sale,J.E. (2010) The Werner's Syndrome protein collaborates with REV1 to promote replication fork progression on damaged DNA. *DNA Repair (Amst)*, **9**, 1064–1072.
33. Szüts,D., Marcus,A.P., Himoto,M., Iwai,S. and Sale,J.E. (2008) REV1 restrains DNA polymerase zeta to ensure frame fidelity during translesion synthesis of UV photoproducts in vivo. *Nucleic Acids Res.*, **36**, 6767–6780.
34. Funk,P.E., Pifer,J., Kharas,M., Crisafi,G. and Johnson,A. (2003) The avian chB6 alloantigen induces apoptosis in DT40 B cells. *Cell. Immunol.*, **226**, 95–104.
35. Funk,P.E., Tregaskes,C.A., Young,J.R. and Thompson,C.B. (1997) The avian chB6 (Bu-1) alloantigen can mediate rapid cell death. *J. Immunol.*, **159**, 1695–1702.
36. Parnes,J.R. and Pan,C. (2000) CD72, a negative regulator of B-cell responsiveness. *Immunol. Rev.*, **176**, 75–85.
37. Webba da Silva,M. (2007) NMR methods for studying quadruplex nucleic acids. *Methods*, **43**, 264–277.
38. Mergny,J.L., De Cian,A., Ghelab,A., Sacca,B. and Lacroix,L. (2005) Kinetics of tetramolecular quadruplexes. *Nucleic Acids Res.*, **33**, 81–94.
39. Mergny,J.L., Phan,A.T. and Lacroix,L. (1998) Following G-quartet formation by UV-spectroscopy. *FEBS Lett.*, **435**, 74–78.
40. Mergny,J.L., Li,J., Lacroix,L., Amrane,S. and Chaires,J.B. (2005) Thermal difference spectra: a specific signature for nucleic acid structures. *Nucleic Acids Res.*, **33**, e138.
41. Dai,J., Dexheimer,T.S., Chen,D., Carver,M., Ambrus,A., Jones,R.A. and Yang,D. (2006) An intramolecular G-quadruplex structure with mixed parallel/antiparallel G-strands formed in the

human BCL-2 promoter region in solution. *J. Am. Chem. Soc.*, **128**, 1096–1098.
42. Heintzman,N.D., Stuart,R.K., Hon,G., Fu,Y., Ching,C.W., Hawkins,R.D., Barrera,L.O., Van Calcar,S., Qu,C., Ching,K.A. *et al.* (2007) Distinct and predictive chromatin signatures of transcriptional promoters and enhancers in the human genome. *Nat. Genet.*, **39**, 311–318.
43. Barski,A., Cuddapah,S., Cui,K., Roh,T.Y., Schones,D.E., Wang,Z., Wei,G., Chepelev,I. and Zhao,K. (2007) High-resolution profiling of histone methylations in the human genome. *Cell*, **129**, 823–837.
44. Litt,M.D., Simpson,M., Recillas-Targa,F., Prioleau,M.N. and Felsenfeld,G. (2001) Transitions in histone acetylation reveal boundaries of three separately regulated neighboring loci. *EMBO J.*, **20**, 2224–2235.
45. Sobel,R.E., Cook,R.G., Perry,C.A., Annunziato,A.T. and Allis,C.D. (1995) Conservation of deposition-related acetylation sites in newly synthesized histones H3 and H4. *Proc. Natl Acad. Sci. USA*, **92**, 1237–1241.
46. Loyola,A., Bonaldi,T., Roche,D., Imhof,A. and Almouzni,G. (2006) PTMs on H3 variants before chromatin assembly potentiate their final epigenetic state. *Mol. Cell*, **24**, 309–316.
47. Houssaint,E., Diez,E. and Pink,J.R. (1987) Ontogeny and tissue distribution of the chicken Bu-1a antigen. *Immunology*, **62**, 463–470.
48. Arakawa,H., Moldovan,G.L., Saribasak,H., Saribasak,N.N., Jentsch,S. and Buerstedde,J.M. (2006) A role for PCNA ubiquitination in immunoglobulin hypermutation. *PLoS Biol.*, **4**, e366.
49. Kee,Y. and D'Andrea,A.D. (2010) Expanded roles of the Fanconi anemia pathway in preserving genomic stability. *Genes Dev.*, **24**, 1680–1694.
50. Kitao,H., Nanda,I., Sugino,R.P., Kinomura,A., Yamazoe,M., Arakawa,H., Schmid,M., Innan,H., Hiom,K. and Takata,M. (2011) FancJ/Brip1 helicase protects against genomic losses and gains in vertebrate cells. *Genes Cells*, **16**, 714–727.
51. Johnson,J.E., Cao,K., Ryvkin,P., Wang,L.S. and Johnson,F.B. (2010) Altered gene expression in the Werner and Bloom syndromes is associated with sequences having G-quadruplex forming potential. *Nucleic Acids Res.*, **38**, 1114–1122.
52. Zee,B.M., Levin,R.S., Dimaggio,P.A. and Garcia,B.A. (2010) Global turnover of histone post-translational modifications and variants in human cells. *Epigenetics & Chromatin*, **3**, 22.
53. Ringrose,L. and Paro,R. (2004) Epigenetic regulation of cellular memory by the Polycomb and Trithorax group proteins. *Annu. Rev. Genet.*, **38**, 413–443.
54. Lehmann,A.R. (1972) Postreplication repair of DNA in ultraviolet-irradiated mammalian cells. *J. Mol. Biol.*, **66**, 319–337.
55. Arakawa,H., Lodygin,D. and Buerstedde,J.M. (2001) Mutant loxP vectors for selectable marker recycle and conditional knock-outs. *BMC Biotechnol.*, **1**, 7.
56. Ambrus,A., Chen,D., Dai,J., Bialis,T., Jones,R.A. and Yang,D. (2006) Human telomeric sequence forms a hybrid-type intramolecular G-quadruplex structure with mixed parallel/antiparallel strands in potassium solution. *Nucleic Acids Res.*, **34**, 2723–2735.
57. Phan,A.T., Kuryavyi,V., Burge,S., Neidle,S. and Patel,D.J. (2007) Structure of an unprecedented G-quadruplex scaffold in the human c-kit promoter. *J. Am. Chem. Soc.*, **129**, 4386–4392.
58. Sonoda,E., Okada,T., Zhao,G.Y., Tateishi,S., Araki,K., Yamaizumi,M., Yagi,T., Verkaik,N.S., van Gent,D.C., Takata,M. *et al.* (2003) Multiple roles of Rev3, the catalytic subunit of polzeta in maintaining genome stability in vertebrates. *EMBO J.*, **22**, 3188–3197.
59. Kawamoto,T., Araki,K., Sonoda,E., Yamashita,Y.M., Harada,K., Kikuchi,K., Masutani,C., Hanaoka,F., Nozaki,K., Hashimoto,N. *et al.* (2005) Dual roles for DNA polymerase eta in homologous DNA recombination and translesion DNA synthesis. *Mol. Cell*, **20**, 793–799.
60. Yamashita,Y.M., Okada,T., Matsusaka,T., Sonoda,E., Zhao,G.Y., Araki,K., Tateishi,S., Yamaizumi,M. and Takeda,S. (2002) RAD18 and RAD54 cooperatively contribute to maintenance of genomic stability in vertebrate cells. *EMBO J.*, **21**, 5558–5566.
61. Wang,W., Seki,M., Narita,Y., Sonoda,E., Takeda,S., Yamada,K., Masuko,T., Katada,T. and Enomoto,T. (2000) Possible association of BLM in decreasing DNA double strand breaks during DNA replication. *EMBO J.*, **19**, 3428–3435.
62. Niedzwiedz,W., Mosedale,G., Johnson,M., Ong,C.Y., Pace,P. and Patel,K.J. (2004) The Fanconi anaemia gene FANCC promotes homologous recombination and error-prone DNA repair. *Mol. Cell*, **15**, 607–620.
63. Bezzubova,O., Silbergleit,A., Yamaguchi-Iwai,Y., Takeda,S. and Buerstedde,J.M. (1997) Reduced X-ray resistance and homologous recombination frequencies in a RAD54-/- mutant of the chicken DT40 cell line. *Cell*, **89**, 185–193.
64. Takata,M., Sasaki,M.S., Tachiiri,S., Fukushima,T., Sonoda,E., Schild,D., Thompson,L.H. and Takeda,S. (2001) Chromosome instability and defective recombinational repair in knockout mutants of the five Rad51 paralogs. *Mol. Cell. Biol.*, **21**, 2858–2866.
65. Okada,T., Sonoda,E., Yamashita,Y.M., Koyoshi,S., Tateishi,S., Yamaizumi,M., Takata,M., Ogawa,O. and Takeda,S. (2002) Involvement of vertebrate polkappa in Rad18-independent postreplication repair of UV damage. *J. Biol. Chem.*, **277**, 48690–48695.
66. Wang,J., Liu,H., Lin,C.M., Aladjem,M.I. and Epner,E.M. (2005) Targeted deletion of the chicken beta-globin regulatory elements reveals a cooperative gene silencing activity. *J. Biol. Chem.*, **280**, 23340–23348.
67. Myers,F.A., Lefevre,P., Mantouvalou,E., Bruce,K., Lacroix,C., Bonifer,C., Thorne,A.W. and Crane-Robinson,C. (2006) Developmental activation of the lysozyme gene in chicken macrophage cells is linked to core histone acetylation at its enhancer elements. *Nucleic Acids Res.*, **34**, 4025–4035.